Simulation of Breast Anatomy: Bridging the Radiology-Pathology Scale Gap

Predrag R. Bakic[1(✉)], David D. Pokrajac[2], Rebecca Batiste[3], Michael D. Feldman[3], and Andrew D.A. Maidment[1]

[1] Department of Radiology, University of Pennsylvania, Philadelphia, PA, USA
Predrag.Bakic@uphs.upenn.edu
[2] Computer and Information Sciences Department, Delaware State University, Dover, DE, USA
[3] Department of Pathology and Laboratory Medicine, University of Pennsylvania, Philadelphia, PA, USA

Abstract. We have developed an efficient simulation of breast anatomy over a range of spatial scales, covering tissue details seen in both radiology and pathology images. The simulation is based on recursive partitioning using octrees, and is performed in two stages. First, the macro- and meso-scale anatomical features are simulated: breast outline, skin, and the matrix of tissue compartments and subcompartments, outlined by Cooper's ligaments. These compartments are labeled as adipose or fibroglandular, according to the desired overall glandularity and the realistic distribution of dense tissue. Second, pathology images are generated to match selected region within the breast, by filling the region with simulated cells (adipocytes, ductal epithelium and myoepithelium, lymphocytes, and fibroblasts) and collagen fibers. Matched synthetic images can support discovery and virtual trials of image-based biomarkers for specific pathology findings. Our proof-of-concept is presented and further optimizations of the simulation discussed.

Keywords: Breast tissue simulation · Virtual clinical trials · Small scale tissue structures · Recursive partitioning · Octrees · Image-based biomarkers

1 Introduction

Computer simulations of breast anatomy have been used for pre-clinical testing of new breast imaging systems and image analysis methods. Breast images synthesized with simulated anatomy are used in virtual clinical trials (VCTs), which have gained significant attention among breast imaging researchers. With the development of digital pathology, and the close relationship between radiology and pathology, there is a growing need for the analysis and simulation of breast anatomy as visualized in radiology and pathology images (Fig. 1).

We have previously developed a method for real-time simulation of breast anatomy at the spatial macro- and meso-scale level [1–3]. Our software breast phantoms and imaging simulation methods have been used by numerous researchers in academia, industry, and government for preclinical trials of digital breast tomosynthesis acquisition

A. Tingberg et al. (Eds.): IWDM 2016, LNCS 9699, pp. 478–485, 2016.
DOI: 10.1007/978-3-319-41546-8_60

Fig. 1. Example of breast tissue sections at various spatial scales, from sub-gross, whole-breast section (left) to digitized histopathological section (right). (*Modified from* [4, 5].)

and reconstruction, image denoising methods, breast density and parenchymal complexity biomarkers, and for the development of anthropomorphic physical breast phantoms.

In this paper we describe the extension of our simulation to the cellular level, and its use to model breast anatomy over a range of spatial scales, from radiology to pathology. Section 2 briefly reviews the histopathology of the breast, identifying the anatomical structures to be simulated. Section 3 describes the simulation method and presents our proof-of-concept results. Advantages and limitations of the proposed method, and further optimization are discussed in Sect. 4.

2 Histopathology of the Breast

Figure 1 illustrates the organization of breast tissue at various spatial scales. Starting from a sub-gross, whole breast section (Fig. 1, left [4]), drawings of magnified tissue sections (Fig. 1, center) show fat compartments (or pearls) and subcompartments (or lobuli) [5], revealing individual cells in a pathology image (a digitized histopathological section, Fig. 1, right). Pathology images show a wide variation in the arrangement of different cell types, as seen in Fig. 2.

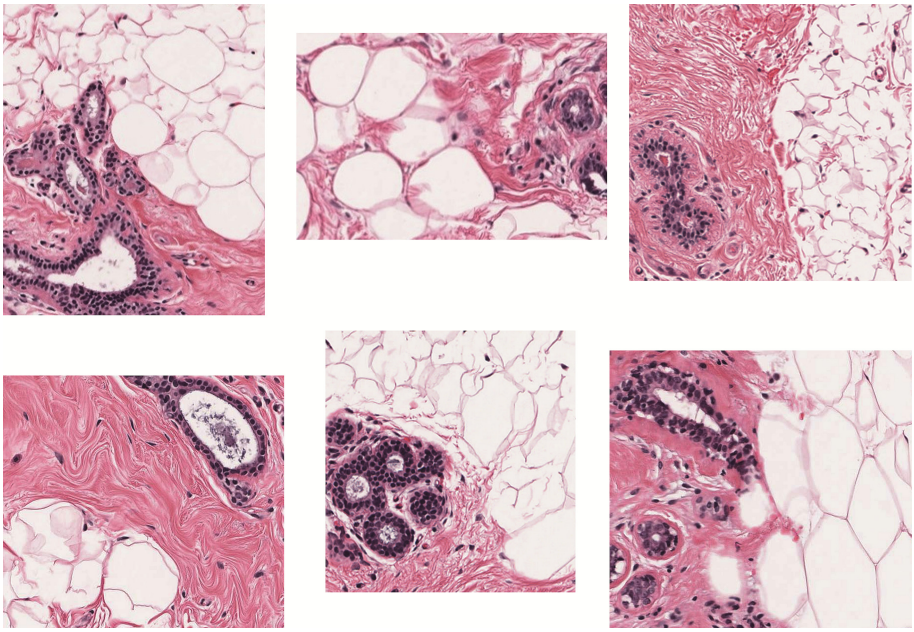

Fig. 2. Details of pathology images (H&E stained), showing regions of predominantly fibroglandular and predominantly adipose tissues.

In this paper, we have focused on the simulation of normal anatomy based upon its description in the literature, and the analysis of pathology images available from the Department of Pathology at the University of Pennsylvania. Simulation of breast abnormalities at the cellular level is our future research task.

Specifically, we simulate the following structures at the cellular scale:

- *Predominantly adipose regions* which consist of *adipocytes* (of size 70–120 μm), hierarchically organized into adipose compartments and subcompartments of decreasing size (*see* Fig. 1, *modified from* [5]), septated by *collagen fiber* ligaments and sparse *fibroblasts cells* (10–15 μm).
- *Predominantly fibroglandular regions* which consist of mammary ducts of irregular shape, lined with two layers of cells: *epithelial* (20–60 μm) and *myoepithelial*; terminal ductal lobular units (TDLUs) with terminal ducts and lobuli/acini (also lined with epithelial and myoepithelial cells), surrounded by basement membrane of *dense and loose fibrous tissue*, with sparse *fibroblast cells* and small *lymphocytes* (7–20 μm).

3 Simulation of the Breast Anatomy at the Cellular Scale

Our breast tissue simulation method is performed in two stages. First, macro- and meso-scale anatomical features are simulated to generate a software breast phantom at *the radiological scale (RS).* This phantom includes the breast outline, a layer of skin, and

the matrix of tissue compartments and subcompartments defined by a hierarchy of Cooper's ligaments [1, 6]. The compartments are labeled as predominantly adipose or fibroglandular, according to the overall breast glandularity, and the realistic distribution of dense tissue [7].

During the second stage, a region within the 3D volume of the RS phantom is selected, and used to simulate the matching pathology image. Figure 3 illustrates the process of selecting the region of the RS phantom to be simulated at the cellular scale.

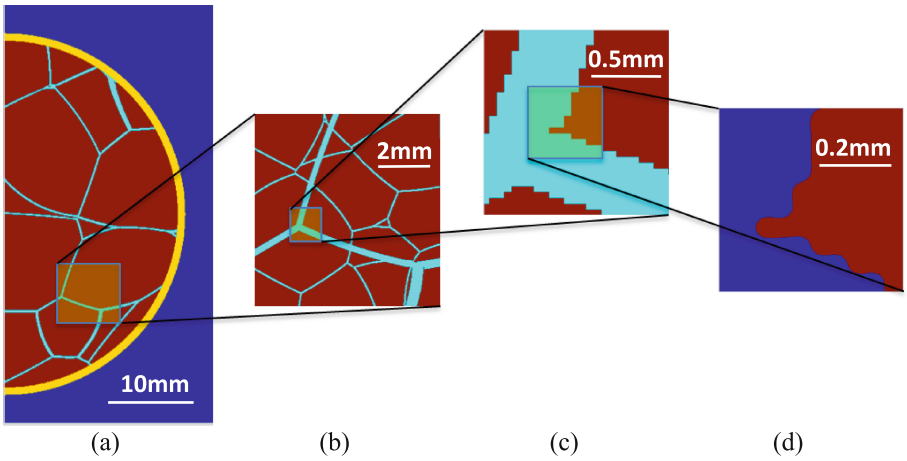

Fig. 3. A desired subvolume (a) within a RS breast phantom is identified and magnified (b and c) to select a small region (d) which will be used as a mask for simulating anatomical structures at the cellular scale.

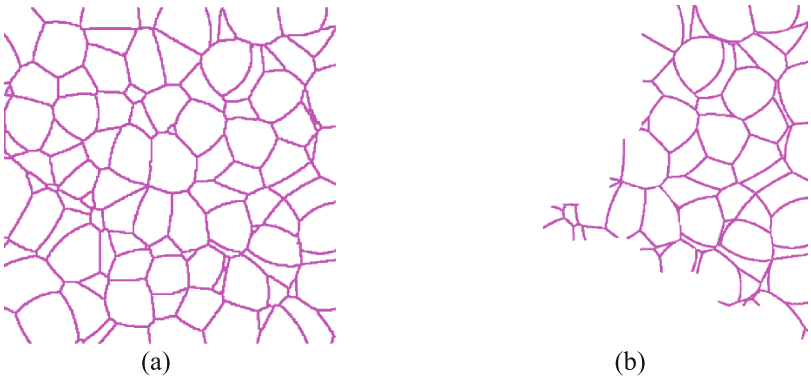

Fig. 4. A random collection of simulated adipocytes (a) is used to fill the adipose region of the matching pathology image (b), based upon the mask extracted from the radiology scale simulation, and resamples to match the pathology scale (Fig. 3(d)).

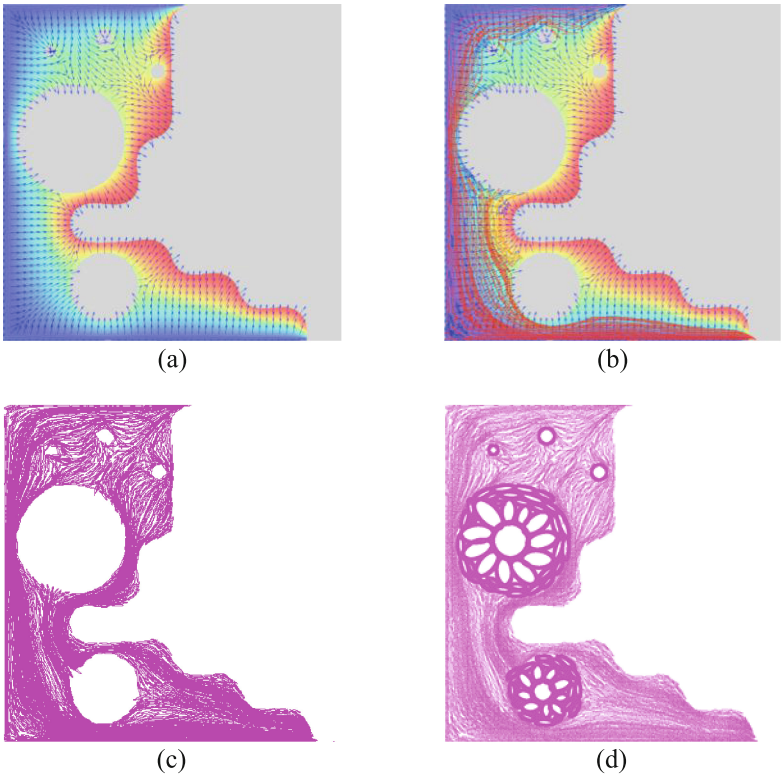

Fig. 5. (a) The region extracted from the RS phantom (Fig. 3(d)), is used for calculating the potential and its gradient to automatically place (b) ellipsoidal fiber bundles and fibroblasts (as illustrated in red) along the equipotential lines. (c) Simulated collagen fiber bundles and fibroblasts. (d) Completely simulated predominantly fibroglandular portion of the pathology image. (Color figure online)

The selected region is resampled to the spatial resolution of the pathology image, and filled with tissue structures simulated at the cellular scale. Appropriate cell types are selected among those listed in Sect. 1. Adipocytes, ductal epithelium and myoepithelium, lymphocytes, fibroblasts and collagen fiber bundles are simulated using recursive partitioning with octrees, [1] selecting appropriate parameters to control the compartment size and shape. Additional anatomical structures may be optionally simulated, e.g., collocated arteries, veins, and lymph vessels, with lumens lined by endothelium, and surrounded by smooth muscles.

For the purpose of this paper, we generated a proof-of-concept example of a pathology image, simulated at 1 μm spatial resolution, starting from an RS phantom simulated at 50 μm voxel size. The region in Fig. 3(d) contains a predominantly adipose portion (part of an adipose subcompartment from the RS phantom), and a predominantly fibroglandular portion (part of a ligament and a glandular tissue from the RS phantom).

The predominantly adipose portion in our example consist of a random collection of adipocytes, simulated using the recursive partitioning in the same fashion as for the adipose compartments of the RS phantom). Figure 4 illustrates the simulation of adipocytes within the predominantly adipose portion of the pathology image.

The predominantly fibroglandular portion consists of a few randomly located ductal segments and/or acini, and lymphocytes, surrounded by fiber bundles and elongated fibroblasts. Figure 5 illustrates the simulation of the predominantly fibroglandular portion of the pathology image. *First*, the locations for each ducts/acini and lymphocyte are selected; the spheroidal lumens of ducts/acini and the extent of lymphocytes are indicated (as light gray spherical areas on the left side of Fig. 5(a)). *Second*, positions and directions of fiber bundles and fibroblasts are automatically selected to follow equipotential lines calculated based upon the following assumptions:

1. The border between the adipose and fibroglandular regions (colored red in Fig. 5(a)) is kept at a given (e.g., positive) potential;
2. The locations of simulated ducts/acini and lymphocytes are kept at the opposite (e.g., negative) potential; and
3. The borders of the selected fibroglandular tissue region (colored blue in Fig. 5(a)) are at zero potential.

The potential values and their gradient are shown in Fig. 5(a) as colored lines and arrows, respectively. Examples of automatically placed fiber bundles and fibroblasts are shown as a connected series of small red ellipses in Fig. 5(b). This method currently does not simulate intracellular structures (e.g., nucleus, cytoskeleton, etc.); thus, our proof–of-concept example does not distinguish between collagen fibers and fibroblasts. Figure 5(b) shows a total of 5,438 simulated ellipsoidal fiber bundles and fibroblasts.

Finally, simulated ducts/acini are added, surrounded by layers of ellipsoidally shaped epithelial cells and flattened myoepithelial cells. Simulating lymphocytes completes the process of filling the predominantly fibroglandular portion of the pathology image, shown in Fig. 5(c).

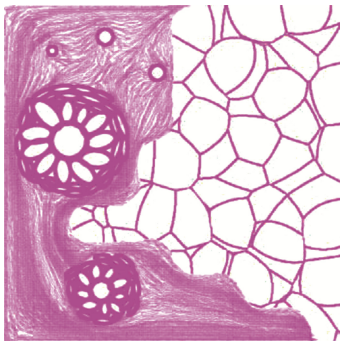

Fig. 6. A simulated pathology image, matching the region selected within the RS software breast phantom (Fig. 3). Included is a random collection of adipocytes (right) and randomly placed lymphocytes (upper left) and ducts/acini (central and lower left) surrounded by fiber bundles and fibroblasts (left). (No cell nuclei are currently simulated.)

Figure 6 shows the final version of the pathology image, produced by combining the simulated predominantly adipose and fibroglandular portions (shown in Figs. 4(b) and 5(c), respectively) of the selected RS phantom region (Fig. 3).

4 Discussion and Conclusions

We have presented a novel method for simulating breast tissue at the cellular level based upon recursive partitioning using octrees. This simulation method can be incorporated with our previously developed software phantoms at the macro/meso-scale, thus bridging the gap between the representation of the breast tissue in radiology and pathology images.

The proof-of-concept example (Fig. 6), shows the cellular scale anatomical structures within a small region selected within a RS breast phantom (Fig. 3). The selected region is extracted, resampled, and used as a mask for simulating predominantly adipose and predominantly fibroglandular tissue portions of the matching pathology image. The simulated tissue portions contain a random collection of adipocytes, as well as randomly placed ductal segments and/or acini, lymphocytes, collagen fiber bundles and fibroblasts. For comparison, Fig. 2 shows details of digitized clinical pathology images from the Department of Pathology at the University of Pennsylvania. Initial visual evaluation of synthetic pathology images has emphasized the realistic appearance of simulated adipocytes, fiber bundles and fibroblasts. A larger observer study by experienced clinical pathologists is currently undergoing.

The approach presented in this proof-of-concept example can be seen as a "zoom-in" of selected regions in the corresponding RS phantoms. For practical purposes, in the example presented it has been assumed that all the cells lay within the same plane of the pathology image. Our recursive partitioning simulation, however, does not require such a limitation; simulated structures (e.g., adipocytes, acini, collagen fibers, etc.) may be positioned at arbitrary 3D locations. This would allow the generation of successive pathology images at different depths, representing 3D pathology matched to the simulated RS phantom. The simulation of the whole breast volume at the cellular scale is not justifiable at the moment, due to the high data storage and transfer requirements. It might be considered, however, with further optimization of our anatomy simulation methods. Alternatively, optimized simulation might allow inclusion of more anatomical detail at the cellular scale (e.g., cell nuclei) to improve the realism of simulated pathology images.

Other directions for future research include the quantification of the spatial distributions for different cell types, corresponding to various parenchymal properties or clinical findings or local variations in breast parenchymal properties, to support realistic simulation of matched radiology and pathology images. Furthermore, the selection of appropriate coloring schemes for the matched pathology images could help represent a range of clinically used stains, for the same simulated cellular anatomy. The presented approach may be extended to simulate breast abnormalities at the cellular scale and enable their visualization in simulated radiological images. Such extended simulation can be used for discovery and virtual clinical trials [8] of image-based biomarkers for specific clinical breast findings.

Acknowledgments. This research was supported by a grant from the U.S. National Cancer Institute (R01 #CA154444), U.S. National Institute of General Medical Sciences (P20 GM103446) from the National Institutes of Health. The work was also supported in part by the US Department of Defense Breast Cancer Research Program (HBCU Partnership Training Award #BC083639), the US National Science Foundation (CREST grant #HRD-1242067), the US Department of Defense/Department of Army (Award #W911NF-11-2-0046). The authors thank Dr. Brad Keller for providing anonymized, previously collected pathology specimen, obtained as part of his Komen Postdoctoral Fellowship.

References

1. Pokrajac, D.D., Maidment, A.D.A., Bakic, P.R.: Optimized generation of high resolution breast anthropomorphic software phantoms. Med. Phys. **39**, 2290–2302 (2012)
2. Chui, J.H., Pokrajac, D.D., Maidment, A.D.A., Bakic, P.R.: Roadmap for efficient parallelization of breast anatomy simulation. In: Physics of Medical Imaging. SPIE, San Diego, CA, pp. 83134T83131–83110 (2012)
3. Chui, J.H., Pokrajac, D.D., Maidment, A.D., Bakic, P.R.: Towards breast anatomy simulation using GPUs. In: Maidment, A.D., Bakic, P.R., Gavenonis, S. (eds.) IWDM 2012. LNCS, vol. 7361, pp. 506–513. Springer, Heidelberg (2012)
4. Wellings, S.R., Jensen, H.M., Marcum, R.G.: An atlas of the subgross pathology of the human breast. J. Nat. Cancer Inst. **55**, 231–273 (1975)
5. Mendieta, C.G.: Power-assisted and ultrasound-assisted liposuction for gluteal sculpting. In: QMP's Plastic Surgery Pulse News. Quality Medical Publishing (2009)
6. Bakic, P.R., Pokrajac, D.D., De Caro, R., Maidment, A.D.: Realistic simulation of breast tissue microstructure in software anthropomorphic phantoms. In: Fujita, H., Hara, T., Muramatsu, C. (eds.) IWDM 2014. LNCS, vol. 8539, pp. 348–355. Springer, Heidelberg (2014)
7. Chui, J.H., Zeng, R., Pokrajac, D.D., Park, S., Myers, K.J., et al.: Two methods for simulation of dense tissue distribution in software breast phantoms. In: Physics of Medical Imaging. SPIE, Lake Buena Vista, FL, pp. 86680M86681–86610 (2013)
8. Maidment, A.D.: Virtual clinical trials for the assessment of novel breast screening modalities. In: Fujita, H., Hara, T., Muramatsu, C. (eds.) IWDM 2014. LNCS, vol. 8539, pp. 1–8. Springer, Heidelberg (2014)